Evaluation of the Role of Metallic Matrix on Environmentally Assisted Embrittlement of Austempered Ductile Iron (ADI) Using High Si Steel

Ricardo A. Martinez

Journal of Materials Engineering and Performance

ISSN 1059-9495

J. of Materi Eng and Perform
DOI 10.1007/s11665-018-3725-8

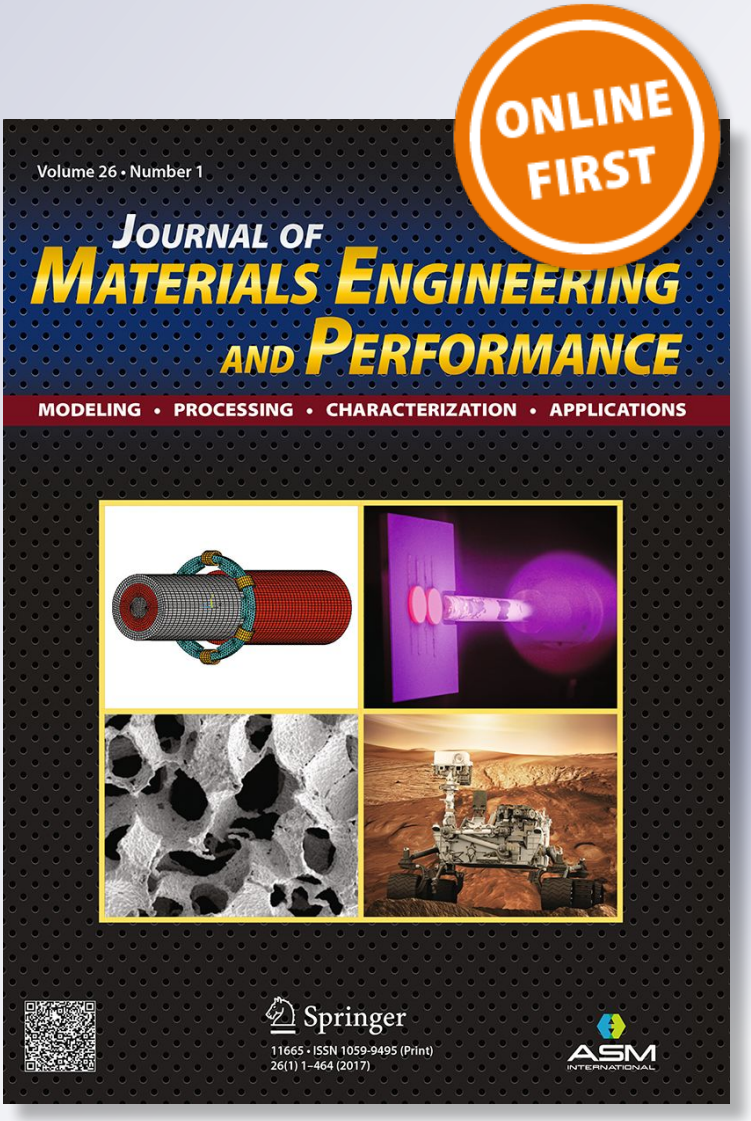

Springer

JMEPEG
https://doi.org/10.1007/s11665-018-3725-8

1059-9495/$19.00

Evaluation of the Role of Metallic Matrix on Environmentally Assisted Embrittlement of Austempered Ductile Iron (ADI) Using High Si Steel

Ricardo A. Martinez

(Submitted November 1, 2017; in revised form August 30, 2018)

The objective of this work stems from the environmentally assisted embrittlement suffered by austempered ductile iron (ADI) when its surface is submerged in water. This phenomenon leads to a drop in elongation and ultimate tensile strength of about 75% and 10%, respectively, while the 0.2% offset strain stress remains unaffected. Heat-treating a high Si steel, an ausferritic matrix similar to that present in the ADI under study is obtained, yielding giving a very good combination of tensile strength and elongation. In this manner, it was possible to examine the influence of the metallic matrix such as that present in ADI, though without nodules and cell boundaries, also called last to freeze zones (LTF). Tensile test evaluations on ADI and steel samples under dry and wet conditions were carried out. Additionally, a very specific test, introducing surface cracks, was conducted with the purpose of expanding the current knowledge on this particular kind of fracture. Earlier investigations on ADI have suggested that the process of embrittlement starts in a surface crack generated at the early stages of plastic deformation in LTF zones, which results from the solidification process, where pores, inclusions and unreacted austenite are present. In this manner, water penetrates and weakens the material strength, making the crack grow very fast and leading to an instantaneous samples failure. The main results obtained in this work include the confirmation of the deleterious effect of the LTF zones in the embrittlement process and the fracture surface analysis showing characteristic features of this kind of failure.

Keywords ADI, embrittlement, steel, water

1. Introduction

Embrittlement phenomena in metallic materials are not exceptional, since different external conditions may exert a detrimental effect on their mechanical properties, thereby reducing plastic deformation capacity, or displacing the ductile–brittle transition temperature, among others. This kind of singularities is attributed to different factors such as operating temperature, surrounding environment and/or the influence of the construction methodology (welding, for example).

For instance, the exposure of the components of 2.25Cr-1Mo steels used in the oil industry for long periods at high temperatures produces a decrease in toughness, which affects service life. This phenomenon is known as temper embrittlement and takes place when the component is exposed to temperatures ranging from 400 to 500 °C for a prolonged period, leading to impurities segregation at grain boundaries (Ref 1).

In this framework, another example is the way in which the surrounding ambient affects material behavior, a phenomenon referred to as environmentally assisted embrittlement (EAE) in the literature. Hydrogen embrittlement has been extensively reported in this regard, which occurs in a wide range of circumstances, including humidity, hydrogen gas and/or hydrocarbon fuels in contact with the material, to name a few (Ref 2, 3).

A different EAE phenomenon that has also been reported is liquid metal embrittlement (LME), which takes place when the surface of a metal is in contact with a liquid metal. This singularity is independent of the exposure time and dependent on the liquid metal that wets the surface.

LME can be observed in several couples such as Cu in liquid Bi, several steels in Pb alloys, Al in liquid Ga and different industrial processes, such as galvanizing. Despite the fact that this phenomenon has long been studied, the mechanisms lying behind it remain unveiled (Ref 4-8).

The focus of this work is placed on EAE, and to be more precise, in those cases in which the cause of embrittlement is the humidity in the material surface found in the environment as vapor or in direct contact with water.

This work was motivated by a research conducted on this type of degradation process on austempered ductile iron (ADI). Even though different aspects have been addressed in order to characterize this particular phenomenon, the decrease in ultimate tensile strength (10%) and elongation (75%) has been conclusive on the effect that the water surrounding the material surface has during uniaxial tensile testing (Ref 9, 10).

It is currently known that a fast fracture process starts at the surface crack generated on a defect present in the material when it is uniaxially tensile loaded and passes through the initial stages of plastic deformation. Water penetrates this crack and weakens the crack tip resulting in very fast propagation and a catastrophic sample failure (Ref 10). A model of chemisorption

Ricardo A. Martinez, Metallurgy Division, INTEMA - UNMDP-CONICET, J. B. Justo 4302 (B7608FDQ) - Mar del Plata, Provincia de Buenos Aires, Republica Argentina. Contact e-mail: rimarti@fi.mdp.edu.ar.

Published online: 02 November 2018

has been proposed to explain this fracture mechanism, but no conclusive evidence of this model has been published as of yet (Ref 11).

The novelty of this work is given by the possibility of finding a high Si steel which upon heat treatment, allows to evaluate the matrix present in ADI avoiding nodules and LTF zones.

ADI is obtained by isothermal heat treatment. A metallic matrix, known as ausferrite, is present, together with graphite nodules that provide excellent mechanical properties and have positioned this material at the very forefront for mechanical components designers.

In addition to ausferrite and graphite nodules, ADI microstructure is also composed of a particular microstructural zone generated at the final stages of the solidification process, which is referred to as ''cell boundary'' or ''last to freeze zone'' (LTF).

This zone presents micro- and macrosegregation patterns (mainly Mn and Si) which promote the presence of inclusions, pores, retained austenite, prone to martensite transformation under strain and carbides. Such presence constitutes a favorable site for cracks generation at the early stages of plastic deformation.

The best results in revealing the solidification microstructure of nodular iron were obtained using a color reagent sensitive to microsegregation (Ref 12), as shown in Fig. 1, where the LTF zones can be clearly distinguished.

The austempering heat treatment commonly used to obtain ADI from a regular ductile iron consists in heating at about 850/900 °C (austenitizing) followed by cooling in a salt bath at temperatures ranging from 250 to 450 °C and holding this temperature for a given period (austempering) ending with the material cooled at air to room temperature.

The resulting metallic matrix comprises a biphasic structure formed of acicular ferrite and carbon-enriched austenite, a microstructure that provides very good plasticity to the material.

When steel is austempered at temperatures under the nose of the time, temperature and transformation curve (TTT), a non-lamellar structure of ferrite and iron carbide is produced. This product with an acicular microstructure is called bainite.

Pearlite is nucleated by iron carbide and is accompanied by ferrite formation. Bainite, in turn, is nucleated by ferrite, and followed by the precipitation of iron carbide. This results in dispersion of iron carbide in the ferritic matrix. The lower the transformation temperature, the finer the carbide distribution with thinner ferrite needles making it possible to distinguish what is commonly referred to as upper and lower bainite.

On the other hand, in steels with 0.4-0.8 of C and sufficient Si addition, cementite formation is inhibited and the microstructure of these alloys results in upper bainite. The carbon that is partitioned into the residual austenite does not precipitate as cementite but remains in site to make the austenite stable at ambient temperature. The microstructure obtained consists of fine plates of bainitic ferrite separated by carbon-enriched regions of austenite quite similar to those described for ADI (Ref 13-16).

Obtaining ausferritic steel by heat treatment with very similar characteristics to those of the ADI matrix offers an alternative to the embrittlement phenomenon under study, since the results of heat-treated high Si steel evaluation will allow analyzing the ADI metallic matrix without nodules and cell boundaries (LTF).

The goal of this work is to evaluate high Si content steel behavior by studying the tensile tests conducted under dry and wet conditions on both materials following the methodology previously applied for ADI assessment (Ref 10, 11).

2. Experimental Procedure

Two materials were used in this work: hot-rolled SAE 9260 steel, commonly used in springs manufacturing, provided in 12.7 mm (0.5 in.) round bars and ductile iron, obtained by pouring a melt on 25 mm Y-block sand molds (ASTM A 536-84) following conventional practices of nodulization, inoculation and cast at the experimental casting laboratory of the Metallurgy Division at INTEMA.

Chemical composition was determined using a BAIRD DV6 optical spark emission spectrometer.

Tensile samples of ADI and steel with threaded grips and a diameter of 6.35 mm in the calibrated section were mechanized (Fig. 2). Before obtaining the final dimensions, samples were heat-treated using electric furnaces and a salt bath.

Austempered ductile iron (ADI) was obtained by heat treatment, consisting in austenitizing for 1 h at 910 °C

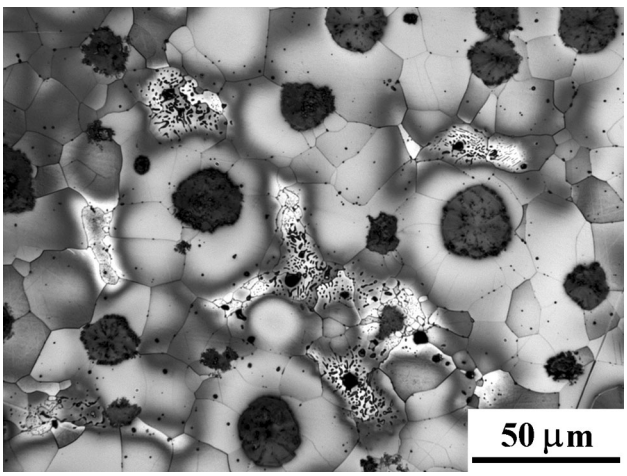

Fig. 1 Last to freeze zones revealed

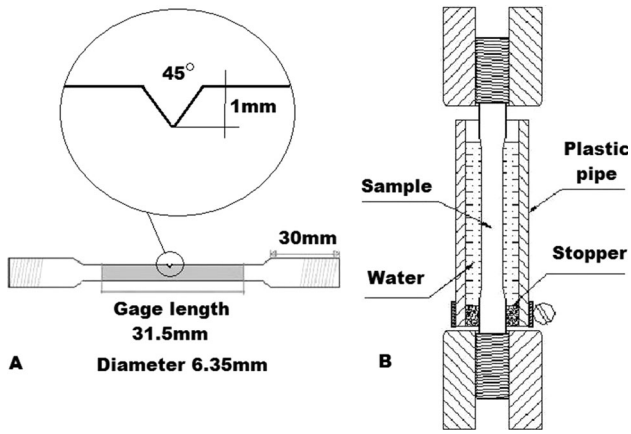

Fig. 2 Samples and experimental setup used for tensile tests

followed by cooling in a salt bath at 360 °C and holding for 1 h and a half (austempering).

As far as the steel is concerned, the heat treatment was determined based on the microstructure observed using several combinations of austenitizing and salt bath temperatures. In this manner, the selected heat treatment for the tensile samples resulted in austenitizing at 880 °C for 1 h followed by an isothermal salt bath treatment at 340 °C also for an hour, ending with the samples submerged in water until room temperature was reached.

In the steel samples group, a 1-mm-deep machined notch with a 45° angle in the calibrated section was prepared in order to introduce a high stress concentrator and so generate artificial cracks (Fig. 2a). Such cracks were obtained by applying cyclic loads to the notched samples using a displacement-controlled mechanical testing machine with a double-eccentric actuator. This condition resulted in a plastic zone extension no greater than 1%. A maximum load of approximately 2.2 kN was applied using a constant eccentricity of $e = 0.145$ mm.

Tensile tests (ASTM E8 M) were conducted using a universal Mohr and Federhaff testing machine in the range of 10 tons maximum capacity at a constant engineering strain rate of 4×10^{-4}., under both dry and wet conditions (submerged samples) using the setup displayed in Fig. 2(b).

Tap water with a pH 7 was used for the wet tests, and they were performed at 20 °C.

Metallographic observations were conducted using an Olympus PGM3 microscope using conventional techniques for grinding and polishing using 2% Nital as the etchant. Scanning electron microscopy (SEM) JEOL JSM-6460LV was used to study the fracture surfaces generated in broken samples.

Hardness measurements ($HBW_{2.5/187.5}$) were performed using an IBERTEST DU 259 universal hardness machine.

X-ray measurements were carried out on a PANalytical X'Pert PRO diffractometer operated at 40 kV and 40 mA using the radiation produced by a copper anode ($k\alpha = 1.542$ Å), performing continuous sweeps covering the interval $2\theta = 38$-86° in steps of 0.05°.

The fraction of retained austenite was determined by comparing the austenite peaks {111, 200, 220} and {200, 112, 022} of ferrite. Austenite quantification was carried out using the ASTM E975 standard.

In all cases, the properties reported were the average value of at least three tests.

3. Results and Discussion

Table 1 lists the chemical composition of the steel and melt used in this work. As regards ductile iron, the average nodular count was 120 nod/mm^2 with a nodularity of 90% and a nodule size 5 according to ASTM A-247 standard. Figure 3 depicts the as-cast microstructure of ductile iron, and Fig. 4 the hot-rolled steel both before heat treatment.

Table 1 Chemical composition of the materials tested (% weight)

s	C	Si	Mn	Cr	Ni	S	P
Steel	0.56	1.47	0.61	0.6	0.04	< 0.003	0.03
Ductile iron	3.58	1.95	0.18	…	0.38	0.02	0.02

Since the main objective of this work is the evaluation of the metallic matrix on the embrittlement phenomenon, it was necessary to adjust the steel microstructure after heat treatment in order to compare it to that found on the ADI under study. With this purpose, several thermal cycles were applied to cylinders 12.7 mm in diameter and 20 mm long.

The equivalence between heat-treated steel and the ADI metallic matrix was evaluated at first using optical microscopy and complementary analysis such as hardness measurements and x-ray tests used to measure the amount of austenite on both materials.

The microstructures of ADI and steel tested samples are displayed in Fig. 5. Steel exhibits a mixture of ferrite and austenite phases similar to ADI.

Hardness values of $320HB_{2.5/187.5}$ were measured on both materials. The x-ray analysis yielded 18% of retained austenite in the metallic matrix of ADI and steel.

Typical x-ray diffraction profile of the austempered samples is shown in Fig. 6.

Once the desired steel microstructure was obtained in agreement with that of the ADI under study, tensile tests were

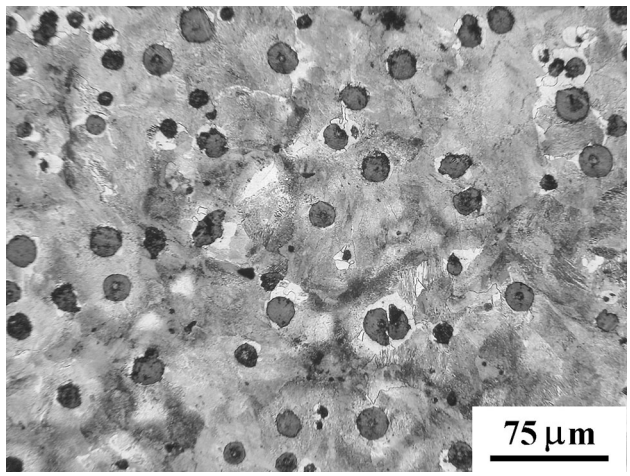

Fig. 3 As-cast microstructure of the ductile iron

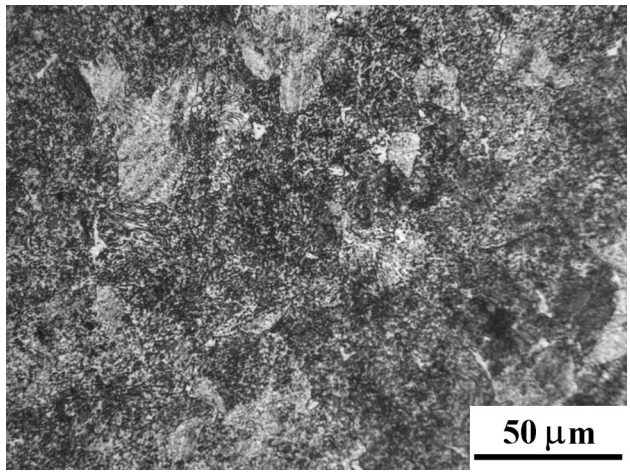

Fig. 4 Hot-rolled steel before heat treatment

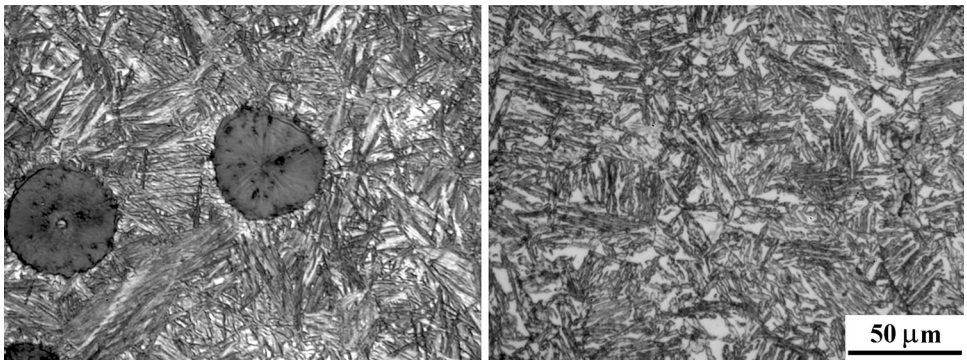

Fig. 5 Microstructures of ADI and austempered 9260 high Si steel

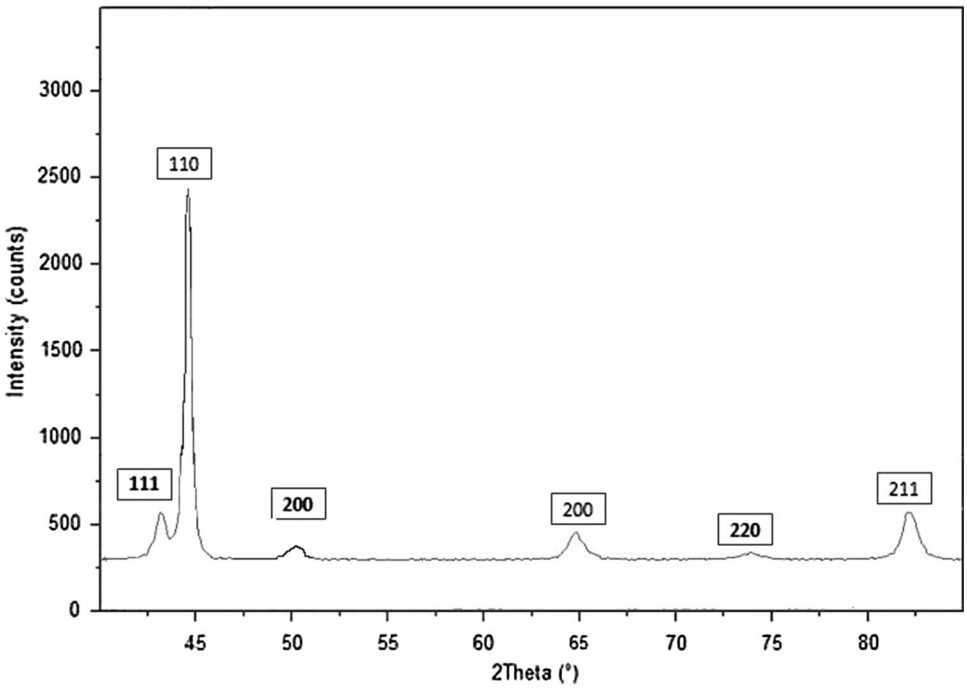

Fig. 6 XRD spectra

Table 2 Tensile properties

Material	Environment	$\sigma_{U.T.S.}$, MPa	$\sigma_{0.2}$, MPa	Elongation, %
SAE 9260 unnotched	Dry	1398	1102	20
	Wet	1386	1095	20.2
SAE 9260 notched	Dry	1234	…	4.7
	Wet	1170	…	2.2
ADI	Dry	1150	881	11
	Wet	987	873	2

Standard deviation is lower than 5.1 in the case of stress and 3.7 for elongation

carried out. Table 2 shows the results obtained for both materials under evaluation, and Fig. 7 displays a load–displacement representative plot.

The environmental effect of water on the surface of ADI is evident, mainly in elongation, as accounted for in earlier research works (Ref 17-21).

In the case of steel, the very good combination of the ultimate tensile strength and elongation in dry conditions can be noticed. Said properties remained unchanged when the samples were tested under wet conditions.

The embrittlement phenomenon of ADI is attributed to the generation of surface cracks at the early stages of plastic deformation (after 0.2% offset strain). The presence of these surface cracks is mainly localized in LTF zones as determined by SEM. The cracks aspect on the lateral surface of the strained sample is illustrated in Fig. 8 (Ref 9, 17, 18).

Figure 9 exhibits the surface of a steel sample exposed to similar conditions, i.e., after the material shortly exceeded yield strength with no evidence of surface cracks, although signs of plastic deformation can be observed.

Cracks formation on ADI surface, preferably at cell boundaries (LTF), is explained by the fact that, in these particular zones segregation is high, leading to carbide presence as well as to defects inherent to castings, such as nonmetallic inclusions and porosity (Fig. 1).

Once a crack nucleates at the surface, the surrounding water penetrates and activates a chemisorption process; the crack tip is weakened and induced to a faster propagation rate, leading to the instantaneous break of the sample.

With the purpose of evaluating the steel behavior under similar conditions, surface cracks were introduced on the samples to simulate the mechanism described for ADI and to compare the results of both materials under equivalent conditions. Even though the crack generated under cyclic load application could be, in some aspects, different to that spontaneously generated in the LTF zones due to the matrix deformation at the initial steps of plastic deformation, the introduction of a sharp crack in the surface is considered an alternative attempt to evaluate the phenomena under study.

Cracks nucleation achieved by applying bending cyclic loads to the calibrated zone with a previously machined notch was monitored observing the notch with a light microscope at 5-min intervals between cyclic load applications until a visible crack appeared.

Figure 10 displays the surface of the machined notch (before) and the crack generated after 45 min as observed by optical microscope.

The samples with cracks generated in this manner were tested in tensile mode. It should be taken into account that UTS and yield strength results were calculated by measuring the remaining ligament area (i.e., the total area of the sample minus the area of the machined notch plus the fatigue crack generated after the sample break).

The results of these comparative tests between steel samples with "artificial" cracks in dry and wet conditions showed that water presence in the crack tip results in a reduction in properties. The most affected one, like in ADI, is elongation (around 50%), while UTS drop is about 10%.

It should be clarified that the results included in Table 2 for cracked steel samples are valid only to compare the effect of a crack simulating the operating fracture mechanism of ADI ("natural cracks" in LTF zones at the initial stages of plastic deformation).

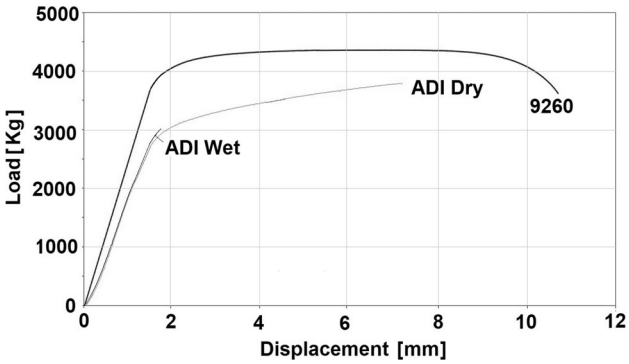

Fig. 7 Representative plot of tensile tests

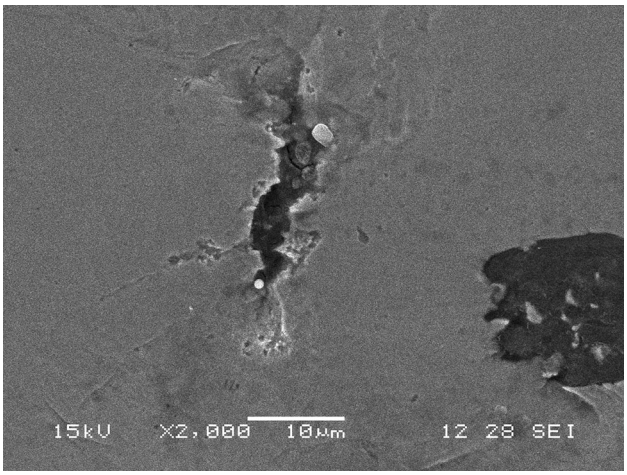

Fig. 8 Surface crack on ADI tensile sample generated at early stage of plastic deformation

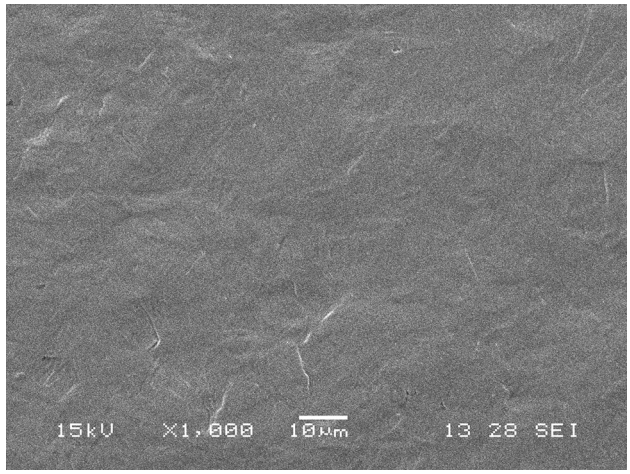

Fig. 9 Surface of steel sample at early stages of plastic deformation

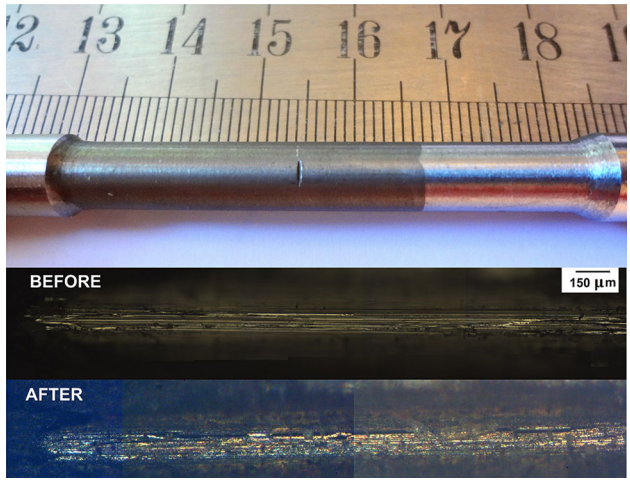

Fig. 10 Machined notch and fatigue crack growth on steel sample

The results obtained in this work allow to conclude that the ausferritic metallic matrix in itself is not responsible for any aqueous environmentally assisted embrittlement.

Since ADI suffers EAE solely with this matrix, it is logical to assume that the phenomenon starts at LTF zones or graphite nodules, thereby confirming the previous results in which cracks generated at initial stages of plastic deformation were located at LTF zones.

At a higher degree of deformation (tested in air), the nodular cavities stretched showing an interstitial space between the matrix and the graphite (Fig. 11).

The last location is not considered as a preferential site for the water embrittlement process to start because, as already stated, these high degrees of plastic deformation are never reached in submerged tested samples.

It is evident that the ausferritic matrix with surface cracks is sensitive to water presence when the sample is tensile loaded. The presence of cracks, "natural" in ADI or "on purpose" in steel, clearly affects the material behavior.

However, elongation reduction in ADI is about 75%, while the reduction in steel with cracks is 50%. This result can be ascribed to the fact that ADI could also have internal cracks (segregated regions) in addition to those observed in the surface and graphite nodules on the fracture path. This fact modifies the fracture mechanism; the steel without these features in its fracture path could be influenced to a lesser degree, sustaining higher plastic deformation.

3.1 Analysis of the Fracture Surfaces

The fracture surface of an ADI sample tested in dry conditions at low magnification is observed in Fig. 12(a). Enlarged nodular cavities and metallic matrix areas with clear signs of plastic deformation such as ridges at the internodular areas and dimples of different sizes and small portions with flat aspect (cleavage) can be noticed. This kind of fracture involves a combination of fracture mechanisms. The failure process begins with microvoids nucleation and second-phase particle growth, such as those present in LTF zones. Small cleavage zones are also detected and probably generated after crack propagation through the cell boundaries where ductility properties are lower than those of ausferrite. This fracture mode is frequently referred to as *quasi-cleavage* (Ref 22, 23).

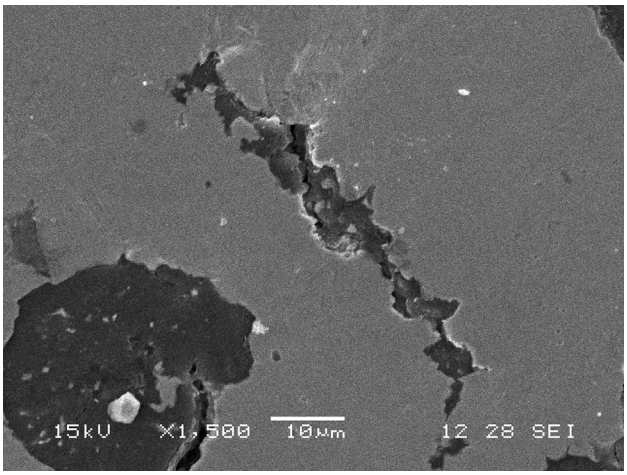

Fig. 11 Nodule cavity opening cracks generated in dry tested ADI sample

Figure 13(a) displays the appearance of the fracture surface when the gage length of the tensile sample is completely submerged in water. Two very different areas can be observed. The figure exhibits a flat area (marked) which has also been described in previous papers as the site where the fracture originates (Ref 19, 22).

This zone, defined as the water-affected zone (WAZ), features a particular propagation mechanism with a cleavage flat aspect, as shown in detail in Fig. 13(b). The fracture mechanism of the cleavage involves breaking bonds. As a consequence, local stress must be enough to surpass the cohesive strength of the material. The susceptibility to start a cleavage fracture is therefore enhanced by water penetration into the material surface defect.

When the WAZ size generated during the initial stage exceeded the critical size, the remaining ligament was unable to endure the applied load and the failure occurred due to overload. The aspect of the remaining surface is similar to that described in the paragraph above for the test conducted in air where the quasi-cleavage mechanism acted.

Even when the microstructure of the ADI metallic matrix and that obtained in the 9260 steel bear many similarities, the differences in the fracture surfaces are very well defined. Needless to say, the presence of graphite nodules and cell boundaries in ADI strongly influences the operating fracture mechanisms in this material.

Figure 14 provides a general view of an austempered 9260 steel sample tested under dry conditions. The fracture progressed with the well-known process of growth and coalescence of voids with the final aspect of cup and cone. Once voids form, further plastic strain and hydrostatic stress cause the voids to grow and finally coalesce.

The central region of the fracture surface has a ductile appearance at low magnifications, which can be better observed in Fig. 14(a). The region in the periphery is relatively smooth, since this surface is oriented 45° from the tensile axis and there is little evidence (at low magnifications) of microvoid coalescence. This type of surface is usually referred to as "shear fracture." Nonetheless, if observed at higher magnification (Fig. 14b), voids with an active role in the fracture process can be noticed.

No differences in the fracture surfaces of samples tested wet were observed. Hence, the paragraph above can be used to define them as well. As a consequence, the mechanical test results showing no water influence on the surface can be confirmed.

Figure 14 depicts the fracture surfaces of notched tensile specimens. The machined notch is observed at the top followed by the crack growth by cyclic load application, with a circular shape. Figure 15(a) corresponds to a sample tested under dry conditions, while 15(b) to a sample submerged in water.

The sample tested in air displays a fibrous fracture after the crack originated by fatigue and follows a radial path with its center in the pre-cracked area. In turn, the submerged sample exhibits a second semicircular zone following the crack generated by the cyclic load. This zone developed under the influence of the water present at the crack tip and applying a monotonic tensile load, by modified assisted crack propagation. This zone features unique characteristics of propagation that differ from those generated by fatigue or overload, and is also referred to as steel water-affected zone (SWAZ) to distinguish it from that observed in ADI.

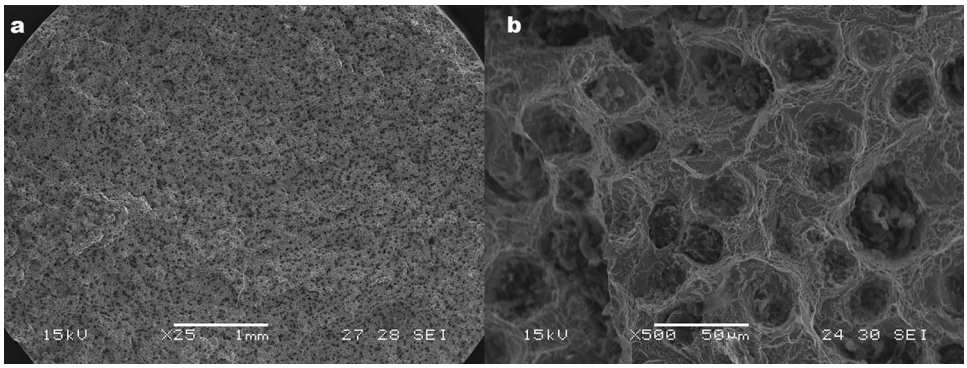

Fig. 12 Fracture surface of an ADI sample tested in dry condition

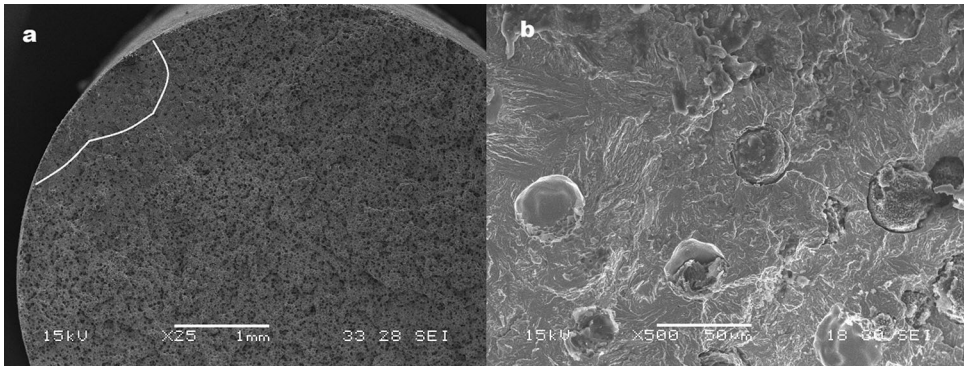

Fig. 13 Fracture surface of an ADI sample tested in wet condition

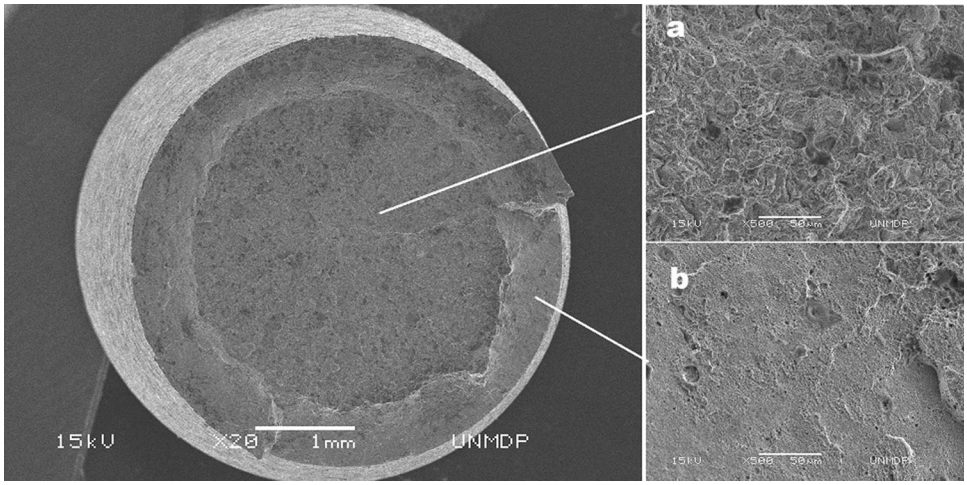

Fig. 14 Fracture surface of steel sample tested in dry condition

The fracture process is completed by different mechanisms, probably due to overload. The different zones are analyzed as follows:

3.2 Steel Water-Affected Zone

SWAZ development occurs under a monotonic tensile load, following the previously generated fatigue crack and influenced by the presence of water at its tip. Figure 16 displays the fracture surface in SWAZ, with characteristics different from those of cyclic load. The particular propagation mechanism features mainly a brittle or quasi-brittle flat aspect proper of cleavage.

The general aspect at low magnification shows a sort of rounded tongues. By increasing the magnification of the image, some voids can be noticed.

This brittle fracture in SWAZ could be related to smaller and more localized strains than those accompanying ductile fractures. Slips occurred on planes intersecting crack fronts, and a faceted surface is observed in SWAZ at the highest magnification, resulting from environmentally assisted cracking under monotonic or sustained loading.

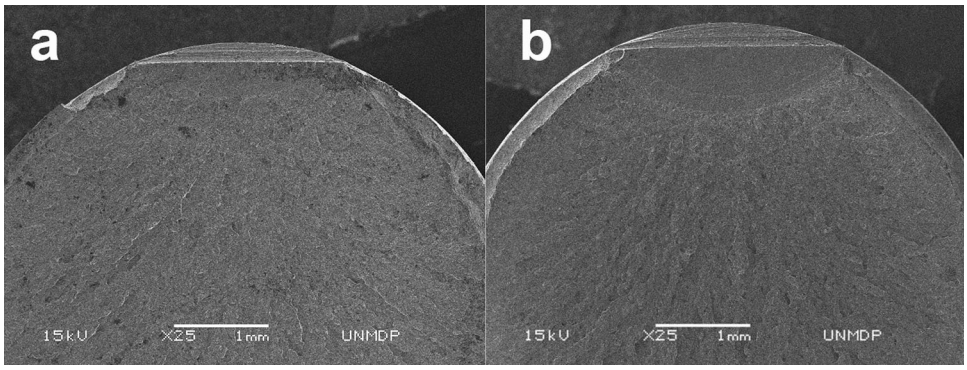

Fig. 15 Fracture surfaces of notched tensile specimens

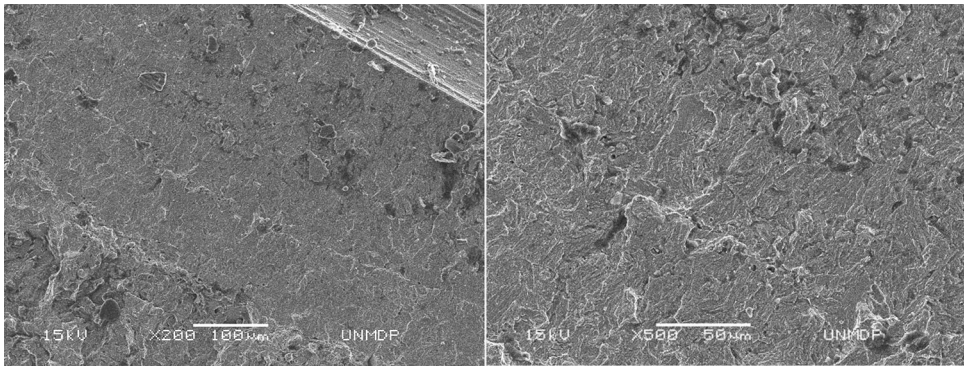

Fig. 16 Steel water-affected zone (SWAZ)

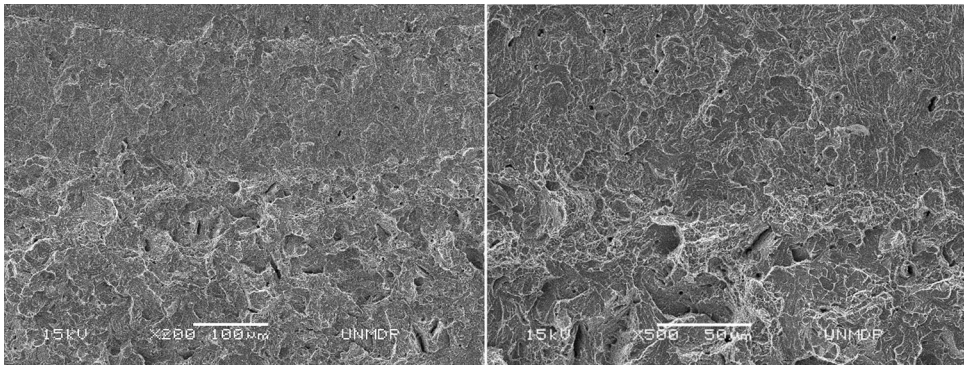

Fig. 17 Steel water-affected zone (SWAZ)

Figure 17 shows SWAZ corresponding to the tested steel at higher magnification, while the WAZ generated on ADI samples is exhibited in Fig. 12(b) both at the same magnification. Undoubtedly, the influence of segregated zones and nodules generates a different fracture surface even with similar metallic matrices of the materials tested.

4. Conclusions

1. It was possible to obtain a microstructure on the 9260 austempered steel which is similar to that of ADI metallic matrix, allowing to evaluate on an isolated basis its behavior avoiding nodules and LTF zones. The very good combination of the ultimate tensile strength and elongation of the selected steel in dry condition can be noticed. Such properties remain unchanged when the samples are tested in wet condition, except in those samples with "artificial cracks."
2. The fact that austempered steel SAE 9260 was not susceptible to the aqueous environmentally assisted embrittlement when the tensile test was conducted with the sample submerged, confirmed that the nucleation of tiny cracks on the LTF present on ADI microstructure is to be blamed for the environmentally assisted embrittlement of ADI and not the ausferritic microstructure.
3. Creating a crack on the steel samples surface to simulate ADI conditions by means of a well-developed technique

used to pre-crack fracture toughness specimens allowed to detect some degree of embrittlement on the steel.
4. The influence of water on mechanical properties is evident when cracks are present on the sample surface, naturally nucleated in ADI or "induced" in 9260 steel.
5. The influence of water on properties drawback in steel samples with surface cracks is less detrimental than that in ADI. This behavior could be attributed to the fact that LTF zones and graphite nodules also participate in the fracture process, thereby emphasizing properties reduction, mainly elongation.
6. A particular fracture surface was detected and referred to as steel water-affected zone (SWAZ), showing unique features when compared, for instance, to fatigue cracks or the overload zone.

Acknowledgments

This work could be the platform for the study of this and other steels, when the load bearing is, for example, of cyclic nature in order to evaluate nucleation and cracks propagation in the presence of water. In addition, the study could be extended to other metallic alloys.

Funding

This study was funded by the National Scientific and Technical Research Council (CONICET)—Grant PIP 0047. The author declares that there is no conflict of interest.

References

1. R.A. Martínez, A. Cassanelli, H. Mejías, J.C. González, B.M. Patchett, and L.A. De Vedia, Development of an AWS E90T1-B3 Type Flux Cored Electrode for Welding 2.25% Cr—1 Mo Steel, *Trends Weld. Res.*, 1989, **1**, p 575
2. G.P. Tiwari, A. Bose, J.K. Chakravartty, S.L. Wadekar, M.K. Totlani, R.N. Arya, and Fotedar, A Study of Internal Hydrogen Embrittlement of Steels, *Mater. Sci. Eng. A*, 2000, **A286**, p 269
3. R.A. Siddiqui and H.A. Abdullah, Hydrogen Embrittlement in 6063 Aluminum Alloy, *J. Mater. Process. Technol.*, 2005, **170**, p 430
4. K. Ina and H. Koizumi, Penetration of Liquid metals into Solid Metals and Liquid Metal Embrittlement, *Mater. Sci. Eng. A*, 2004, **387**, p 390
5. R.E. Clegg and D.R.H. Jones, Liquid Metal Embrittlement of Tensile Specimens of En19 Steel by Tin, *Eng. Fail. Anal.*, 2003, **10**, p 119
6. T. Auger and G. Lorang, Liquid Metal Embrittlement Susceptibility of T91 Steel by Lead–Bismuth, *Scr. Mater.*, 2005, **52**, p 1323
7. E. Izumoto and R. Nishimura, Failure analysis of a Weld-Decayed Austenitic Stainless Steel, *Corros. Sci.*, 2011, **53**, p 886
8. X. Gong, P. Marmy, L. Qin, B. Verlinden, M. Wevers, and M. Seefeldt, Effect of Liquid Metal Embrittlement on Low Cycle Fatigue Properties and Fatigue Crack Propagation Behavior of a Modified 9Cr–1Mo ferritic–Martensitic Steel in an Oxygen-Controlled Lead–Bismuth Eutectic Environment at 350°C, *Mater. Sci. Eng. A*, 2014, **618**, p 406
9. S. Komatsu, C.Q. Zhou, S. Shibutani, and Y. Tanaka, Embrittlement Characteristics of Fracture Toughness in Ductile Iron by Contact with Water, *Int. J. Cast Metals Res.*, 1999, **11**, p 539
10. R.A. Martínez, R. Boeri, and J.A. Sikora, Embrittlement of Austempered Ductile Iron Caused by Contact with Water and Other liquids, *Int. J. Cast Met. Res.*, 2000, **13**, p 9
11. B. Laine, S.N. Simison , R.A. Martínez, R. Boeri, Anales del congreso CONAMET/SAM—SIMPOSIO MATERIA., Santiago de Chile, Chile, 2002, (1), p. 121
12. G. Rivera, R. Boeri, and J. Sikora, Revealing the Solidification Structure of Nodular Iron, *Int. J. Cast Met. Res.*, 1995, **8**(1), p 1–5
13. H.K.D.H. Bhadeshia, *Bainite in Steels*, 2nd ed., IOM Communications Ltd, London, 2001
14. J.L. Páez, F. Fuentes, and A. Battagliese, Tratamiento isotérmico de los aceros aleados al silicio Tipo SAE 92XX, *Rev. Metal. Madrid.*, 1996, **32**, p 3
15. N. Tsuji, M. Ayada, T. Takashima, and Y. Saito, Ausformed Bainite in SUP7 Spring Steel, *Tetsutihagane*, 1999, **85**, p 419
16. S.K. Putatunda, A.V. Singar, R. Tackett, and G. Lawes, Development of a High Strength High Toughness Ausferritic Steel, *Mater. Sci. Eng. A*, 2009, **513–514**, p 329–339
17. R.A. Martínez, S. Simison, R. Boeri, *Crack Initiation in Austempered Ductile iron Strained in Contact with Different Liquids, Science and Processing of Cast Iron*, 2006, vol 1. p 145–150
18. L. Masud, R.A. Martínez, S. Simison, and R. Boeri, Embrittlement of Austempered Ductile Iron on Contact with Water—Testing Under Applied Potential, *J. Mater. Sci.*, 2003, **38**, p 2971
19. L. Caballero, M. Elices, and R.N. Parkins, Environment-Sensitive Fracture of Austempered Ductile Iron, *Corrosion*, 2005, **61**, p 51
20. D. Rajnovic, S. Balos, L. Sidjanin, O.E. Cekic, and J.G. Novakovic, Tensile Properties of ADI, Material in Water and Gaseous Environments, *Mater. Charact.*, 2015, **101**, p 26
21. R.A. Martinez, Fracture Surfaces and the Associated Failure Mechanisms in Ductile Iron with Different Matrices and Load Bearing, *Eng. Fract. Mech.*, 2010, **77**, p 2749
22. G.L. Greno, J.L. Otegui, and R. Boeri, Mechanism of Fatigue Crack Growth in Austempered Ductile Iron, *Int. J Fatigue*, 1999, **21**, p 35
23. S. Lynch, Ductile and Brittle Crack Growth: Fractography, Mechanisms and Criteria, *Mater. Forum*, 1988, **11**, p 268